Optical measurements association using optimized boundary value initial orbit determination coupled with Markov clustering algorithm

Carlos Yanez, Juan Carlos Dolado Pérez, Pascal Richard, Ivan Llamas, Laurent Lapasset

OPTICAL MEASUREMENTS ASSOCIATION USING OPTIMIZED BOUNDARY VALUE INITIAL ORBIT DETERMINATION COUPLED WITH MARKOV CLUSTERING ALGORITHM

C. Yanez[(1)], J-C. Dolado[(1)], P. Richard[(1)], I. Llamas[(2)], and Laurent Lapasset[(3)]

[(1)]*CNES, 18 av. Edouard Belin, 31401 Toulouse Cedex 9, France, Email: carlos.yanez@cnes.fr*
[(2)]*GMV Innovating Solutions, 17 rue Hermès 31520 Ramonville St. Agne, France*
[(3)]*ENAC, 7 avenue Edouard Belin, 31000 Toulouse, France*

ABSTRACT

Identification of new circumterrestrial space objects is essential for building up and maintaining a catalogue of resident space objects (RSO). It is a recurrent task that we have to deal with in a day-to-day catalogue maintenance and that will become more intensive with the increasing awareness on space debris risks as more sensors get dedicated to the space surveillance effort. Robust algorithms are therefore needed in order to envisage automatic measurements associations that enable us to process large quantities of sensors data. This paper addresses this problem combining a method for optical tracklets association [1] with a clustering method [7] used in big data problems. Performance of this approach is assessed in real scenarios using measurements taken by a ground based robotic telescope located at Chile that belongs to the TAROT (Rapid Response Telescopes for Transient Objects) network.

Key words: Space Debris; Correlation; Optical Measurements; Graph Clustering.

1. INTRODUCTION

One of the main missions of Space Surveillance is the detection and cataloguing of space objects. Maintenance of this catalogue is fundamental in order to enable the database to be used for, among others, collision risk assessment and reentry analysis. This maintenance comprises a twofold task. On one hand, it is necessary to keep track of known objects and reduce the uncertainty on their state vector. On the other hand, catalogue is expected to be enriched with objects that either were not identified up to then or coming from already catalogued object that have endure a fragmentation event (collisions or explosions). Tackling the latter problem is the scope of this paper. Of special interest is the case concerning close objects (originated from a recent fragmenation, or belonging to a cluster of satellites), for which identification can be messy and robust methods are therefore needed.

Association of uncorrelated tracks and initial orbit determination is essential in the cataloguing task and, for this reason, it has been the object of intense research in recent years. Siminski et al [1] have developed a method based on a boundary value formulation. It uses the solution of the Lambert's problem to calculate orbit candidates which are then discriminated comparing angular rates by means of the Mahalanobis distance. One of the advantages of this Optimized Boundary Value Initial Orbit Determination (OBVIOD) method compared to others is a less sensitivity in orbit accuracy with respect to measurements noise. We can then apply this method to the identification of new objects [2], processing each possible combination of two uncorrelated tracklets in order to give a likelihood score based on the loss function (the Mahalanobis distance), and those pairs with a score below a predefined threshold are filtered out as a true association. However, we cannot guarantee the absence of false associations among the filtered pairs. These false associations, usually coming from observations of close objects, will prevent the correct distinction between objects and, in this way, a synthetic object generated from observations of several real objects will come up from computations with a high risk of not being able to correlate to future observations. Novelty of the present work consists of introducing the notion of graph to store the correlations relationships and applying to this graph the Markov clustering algorithm to tackle the problem of false associations. This approach leads to a more robust distinction between different objects observed, specially the clustered ones.

Performance of this approach is investigated by means of simulated observations concerning three objects in geostationary orbit (GEO). This work includes analysis on the accuracy of the estimated orbit, observation residuals and association goodness-of-fit. Moreover, an analysis is presented processing a real set of optical measurements taken by French TAROT telescope located at Chile [4] that comprises a sky region where a cluster of three colocated GEO satellites are orbiting. All the analysis and results presented in this paper have been performed using *BAS*^{3}*E*, the CNES tool which simulates a whole space surveillance system.

2. OPTIMIZED BOUNDARY VALUE INITIAL ORBIT DETERMINATION (OBVIOD)

The Boundary Value method developed in [1] is used in this study to compute an association probability between two tracklets, as well as to have an initial estimate of the orbit that best fits these two tracklets. Hereafter, a brief description of the method is presented along with some results concerning the precision of the method and considerations on the way it is used.

2.1. Method Description

The OBVIOD method deals with the association of optical observations. Optical sensors provide a series of close images (very short arc), each image containing, at an epoch t, an observation composed of a pair : right ascension α_t and declination δ_t of an object. A series of observations forms a *tracklet* if they all belong to the same object. This *correlation* inside a tracklet is performed by simple linear correlation algorithms. Hence the importance that the series of images are close enough, so that they can be unambiguously fit. In the case of TAROT telescopes, a tracklet is made of three observations separated 20 s, each observation subject to a noise of 1 arcsec in both angular coordinates. The advantage of leading with tracklets instead of with individual observations lies in the fact that we can make use of angular rates. Within this study, angular rates are always computed by fitting a linear regression from a series of three observations. Equivalently, angular coordinates are taken directly from the linear fit as the value at the central epoch of the tracklet. Raw values of any particular observation are, therefore, not used. The information contained in a tracklet is compressed into an attributable vector [3] at epoch t in the following form:

$$\bar{A}_t = (\alpha, \dot{\alpha}, \delta, \dot{\delta})_t^T, \tag{1}$$

Following [11], measurement noise associated to this attributable can be approximated to:

$$\sigma_\theta^2 = \frac{1}{N}\sigma_{\theta_{raw}}^2, \tag{2}$$

$$\sigma_{\dot{\theta}}^2 = \frac{12}{\Delta t^2 N}\sigma_{\theta_{raw}}^2, \tag{3}$$

where θ is either the right ascension or the declination, N is the number of measurements contained in the tracklet and Δt the separation between observations.

The boundary value problem formulation is built up from the angular coordinates of the tracklets at both observation epochs:

$$\bar{z} = (\alpha_1, \delta_1, \alpha_2, \delta_2)^T, \tag{4}$$

Orbital state is completely defined with hypotheses on the range at t_1 and t_2. We form then a hypothesis variable denoted as $\bar{p} = (\rho_1, \rho_2)$, that permits us to define the position vectors and, therefore, a Lambert's problem. Lambert's problem refers to the orbital boundary value problem constrained by two position vectors and the elapsed time ($dt = t_2 - t_1$, in this case). We also need to specify the number of complete revolutions made during the transfer, k. In this work, solution of the Lambert's problem is obtained by the method developed in [5]. The orbit solution permit us to obtain computed angular rates :

$$\hat{\dot{\bar{z}}} = (\hat{\dot{\alpha}}_1, \hat{\dot{\delta}}_1, \hat{\dot{\alpha}}_2, \hat{\dot{\delta}}_2)^T. \tag{5}$$

Notice that the hat variables refer to *computed* values in contrast to non-hat variables ($\bar{z}$ and $\dot{\bar{z}}$) that refer to *observed* values. Each possible hypothesis $\bar{p}$ leads to a different Lambert's problem and, consequently, to a different candidate orbit. The quality of a candidate orbit is evaluated by assessing the agreement between computed and observed angle rates. An optimization scheme is then followed to obtain the best candidate orbit, $\bar{p}^*$, based on the minimization of a loss function defined as follows:

$$L(\bar{p}, k) = (\dot{\bar{z}} - \hat{\dot{\bar{z}}})^T \bar{C}^{-1} (\dot{\bar{z}} - \hat{\dot{\bar{z}}}), \tag{6}$$

where $\bar{C}$ is a covariance matrix that accounts for the uncertainties on both the observed and the computed angular rates. This loss function represents the Mahalanobis distance between $\dot{\bar{z}}$ and $\hat{\dot{\bar{z}}}$. A characteristic of this distance is that it is distributed according to a χ^2 distribution. Tracklet information is used in a twofold way:

1. *Angular coordinates* are used to define candidate orbits. Each candidate orbit is the solution of a Lambert's problem under range hypotheses constraints.
2. *Angular rates* are used to discriminate the most suitable orbit among all candidate orbits.

The $(\bar{p}, k)$-space is not considered unbounded for the optimization search, but, on the contrary, some constraints are imposed in the orbital elements depending on the type of object we can encounter. This entails the definition of a compact subset, also known as *admissible region* [3]. We follow [1] and define the admissible region in terms of allowed semi-major axis interval (a_{min}, a_{max}) and greatest allowed eccentricity, e_{max} . This leads to the following allowed range interval:

$$\rho_{min,i} = -c_i + \sqrt{c_i^2 + r_{min}^2 - r_{s,i}^2}, \tag{7}$$

$$\rho_{max,i} = -c_i + \sqrt{c_i^2 + r_{max}^2 - r_{s,i}^2}, \tag{8}$$

where i is an index that stands for the first or second tracklet, r_s is the norm of the sensor position, c is the dot product between sensor position and line-of-sight, and the allowed radius interval is defined as follows:

$$r_{min} = a_{min}(1 - e_{max}), \tag{9}$$

$$r_{max} = a_{max}(1 + e_{max}). \tag{10}$$

Additionally, the constraint on the semi-major axis also defines bounds on the allowed interval of orbital revolutions:

$$k_{min} = \lfloor dt/P(a_{max}) \rfloor, \tag{11}$$

$$k_{max} = \lfloor dt/P(a_{min}) \rfloor, \tag{12}$$

where $P = 2\pi\sqrt{(a^3/\mu)}$ is the orbital period from Kepler's third law.

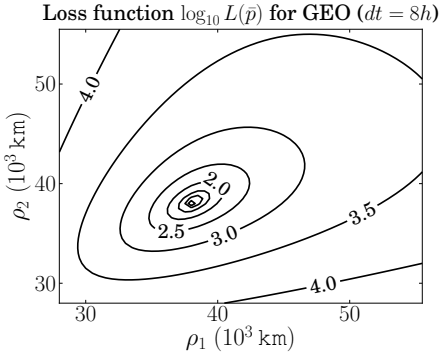

Figure 1: Loss function for a GEO object in the case of tracklets separated by 8 hours

2.2. Loss Function Topography

The topography of the loss function in the p-hypotheses space should be sufficiently smooth in order to succeed in the function minimization and, in consequence, in finding the hypothesis that better fits the observations. This minimization is performed verifying some inequality constraints that defines the admissibility region. Techniques of convex optimization [10] are used, requiring twice continuously differentiable multivariate real functions. We have performed extensive simulations for a GEO object to assess the sensibility of the loss function topography against separation between tracklets. Tracklets are composed of three consecutive images separated 20 s containing angular measurements of 1 arcsec centered Gaussian noise. The admissible region is defined under the following constraints : $40000 < a[km] < 50000$ and $e_{max} = 0.2$. This admissible region is used all along this work in the case we look for near-geostationary objects. In general, the loss function is smooth enough as we can see in Figure 1. Nevertheless, we have encounter two situations where topography deformation complicates the problem:

1. Exact number of orbital periods separation. In the vicinity of exact number of revolutions the loss function begins to become deformed (see Figure 2a), until it gets completely stretched (see Figure 2b) and, in consequence, no optimization can be performed. This *singularity* is not specific to GEO orbits, but we have found the same behaviour in other orbital regimes (highly elliptical and medium earth orbits). We claim that this feature shall be taken into account as a constraint in the definition of surveillance strategies. If, for example, we are intended to survey the geostationary ring, employing this method implies, in consequence, to prevent looking at the same longitude bands at the same hour every night.

2. Regions with no solution of Lambert's problem. There is a maximum number of revolutions for transfer between two tracklets given a hypothesis $\bar{p}$. In the optimization scheme, we look for a minimum of the loss function for each $k \in (k_{min}, k_{max})$. In that way, we apply optimization techniques to a problem with a fixed k. For a given k, it is possible that a solution to the Lambert's problem exists, within the admissible region, for a set of $\bar{p}$-hypotheses but not for others. This is the case of Figure 2c where a chaotic region can be seen. This region corresponds to the set of $\bar{p}$-hypotheses for which no solution exists for $k = 1$ and, consequently, the Lambert solver does not converge. In those cases where no convergence is found, we jump to the solution for $k - 1$. This prevents the optimizer to fail, and, in doing so in our example, the loss function topography passes from Figure 2c to Figure 2d enabling the global minimum to be found.

2.3. Orbit precision

One of the reasons of having selected the OBVIOD method for linkage is the precision in the initial orbit obtained and, in particular, the stability against measurement noise. Figure 3 (left) shows the accuracy of the orbit depending on the separation of the two tracklets. It is worth noting the increase of accuracy on the semi-major axis for longer intervals, and the typical concave shape for the eccentricity with a minimum around half an orbital period. This indicates that we should favor tracklets separated as much as possible in one night or belonging to two consecutive nights. Figure 3 (right) presents the sensitivity of the solution against measurement noise, it is worth noting the nearly linear relation between accuracy and noise, which is evidence of the robustness of the OBVIOD method.

3. MARKOV CLUSTERING ALGORITHM

The OBVIOD method states that a pair of tracklets is correlated if the minimum of the loss function, $L_{min} = L(\bar{p}^*, k^*)$, lies below a predefined threshold. Passing the threshold gate, then, means correlation. For object identification, we only consider those pairs that pass the threshold gate. By doing so, we can handle pairs that are actually correlated but we can also face the case of a false positive correlation (see Table 1). Definition of this threshold stays somehow subjective and conditioned on two opposite types of reasoning : either we take a quite low threshold to try to process only true positive correlations with the drawback of considering few tracklets of the total, or we take a higher threshold to process more pairs, increasing, at the same time, the number of false positives. In a real case, especially when objects are too close (for example, with co-located geostationary satellites, or few time after a fragmentation event) we cannot guarantee the absence of false positives. The reason why true and false positives can have similar values of the loss function is mainly due to, both, the measurement noise, and the dynamical model simplification in the Lambert's problem solution.

Only one false positive would lead to grouping tracklets from two different objects into one *identified* object with

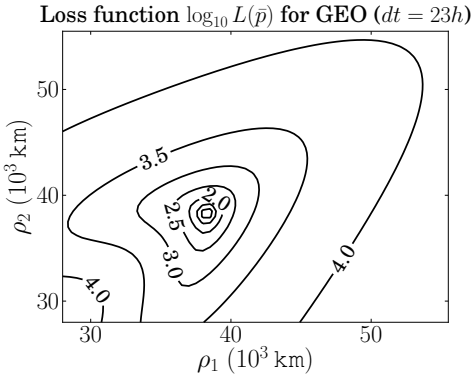

(a) Minimization is still possible

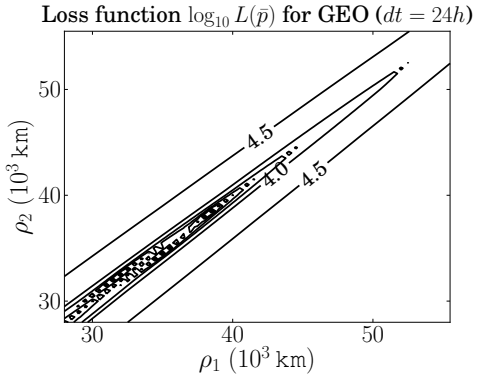

(b) Stretched topography preventing minimization

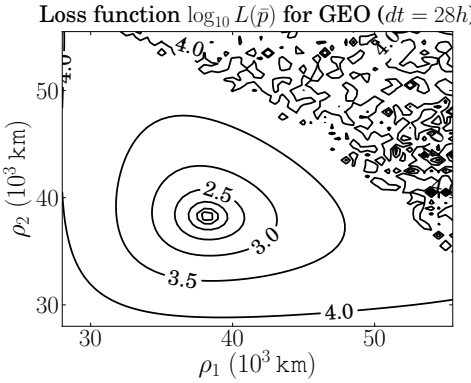

(c) Solution $k = 1$. The upper right triangle of the figure (*chaotic regions*) has no Lambert solution for one complete revolution.

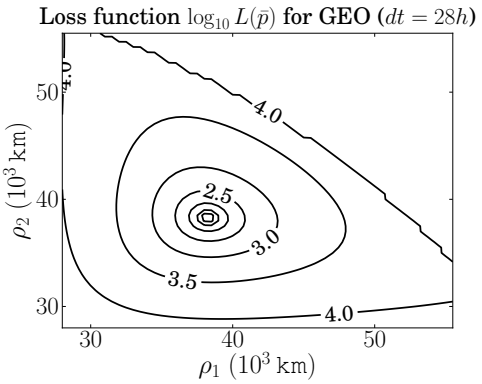

(d) Solution $k = 1$, except for the previous *chaotic* region where a value $k = 0$ is taken.

Figure 2: Loss function topography difficulties.

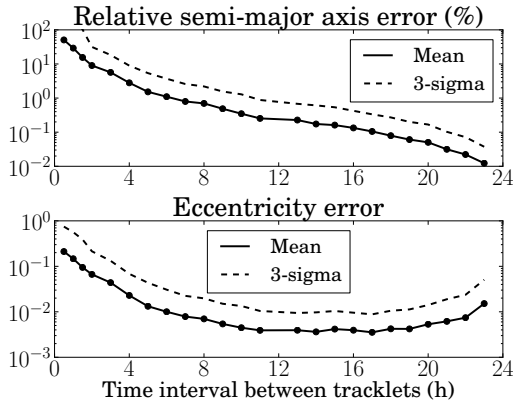

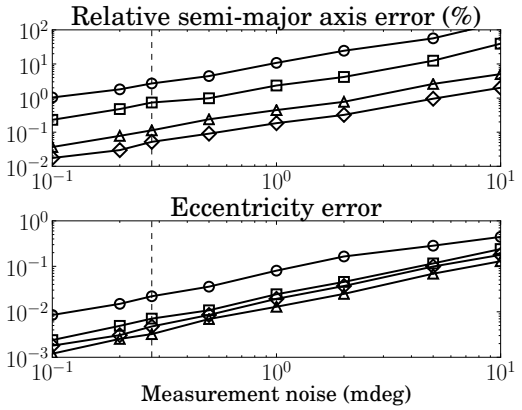

Figure 3: Precision of OBVIOD method for a GEO object as a function of the separation between tracklets (left) and as a function of the sensor noise (right). Left: Measurement noise is 1 arcsec in both angular coordinates. Right : Circle markers correspond to 4 hours separation between tracklets, squares to 8 h, triangles to 16h and diamonds to 20h. Statistical values are computed from a sample of 100 executions

	Test says "Correlation"	Test says "Not correlation"
Correlation	**True positive**	False negative
Not correlation	**False positive**	True negative

Table 1: Possibilities in gating association

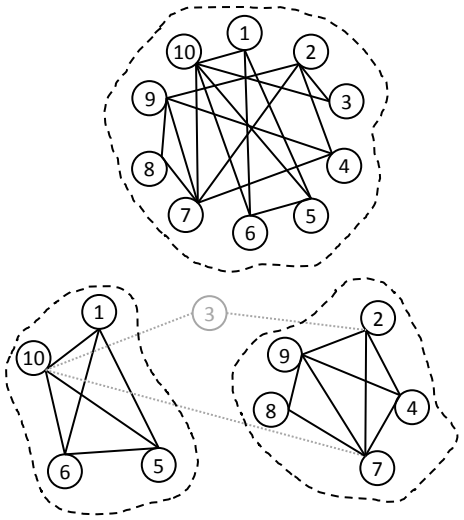

Figure 4: Top: A graph representing one only cluster. Circles are nodes (tracklets) and lines are edges (correlation relationships). Bottom: Same graph split into two clusters with the Markov Clustering algorithm using an inflation parameter $\in (1.5, 3.5)$

the clear risk of not being able to recover it in subsequent observations. Dealing with this problem is therefore essential in object identification.

3.1. Graph construction

A *graph* is a mathematical structure formed by a set of objects, usually called *nodes* or *vertices*, that can be related in one-to-one relationship via *edges*. In this work, nodes correspond to the tracklets and edges correspond to the correlation gating test (1 if the pair passes the test or 0 otherwise). Order of tracklet in the pair has no incidence in the correlation relationship. Thus, we speak of *undirected graphs*, in contrast to directed graphs where the sense of the relationship does play a role. Graphs can be represented as a matrix, where columns and rows refer to tracklets and the element (i, j) of the matrix to the relationship between tracklets i and j. Such a matrix is symmetric in the case of undirected graph.

3.2. Graph clustering

Graph clustering is a field of intense research, especially with the advent of *big data*, that aims to recognize *communities* from a large amount of data [6]. These communities or *clusters* are characterized by having many edges within their nodes, and few edges with nodes of other clusters. In our case of study, these clusters correspond to the set of tracklets defining one object and the few edges between clusters the false positives. Representing our problem is such a way assumes implicitly the following:

- A sufficiently great amount of observations are processed in order to big data techniques apply.
- A relative low threshold of the loss function is set and, in that way, false positives are scarce compared to true positives.

One popular graph clustering method is the Markov Clustering (MCL) algorithm developed in [7], that have been successfully used in different domains as protein families identification in biology [8] or lexical acquisition and word sense discrimination [9]. Markov Clustering partitions a graph via simulation of random walks. The idea is that random walks on a graph are likely to get stuck within dense subgraphs rather than shuttle between dense subgraphs via sparse connections. This approach results in a sequence of algebraic matrix operations (normalization, expansion in powers and inflation) that converges in such a way that inter-cluster interactions are eliminated and only intra-cluster parts stay. Three parameters have to be specified in the MCL algorithm : self-loop, power and inflation parameters. Self-loop parameter indicates if there is a relationship of each node with itself. In this study, self-loops are considered, meaning that in the matrix representation of the graph all the diagonal elements are set to 1. Also, the power parameter is set to 2, that is to say, in the expansion step we always take the square of the matrix. The only parameter which is not fixed within this study is the inflation parameter. This parameter affects the granularity of the solutions (see [7]). The higher this parameter is, the denser and smaller are the clusters of the solution.

3.3. Use of clustering in object identification

Our approach can be summarized in the following steps:

1. Application of the OBVIOD method to all possible combinations of two tracklets (except those at the same epoch) with a correlation gating test defined by a threshold L^* for L_{min}.

2. Building up the associated matrix representing the graph where nodes are tracklets and edges are set to 1 if it relates nodes that have passed the gating test (correlated) or 0 otherwise (not correlated).

3. Application of Markov clustering algorithm to the previous graph. Identified clusters correspond to tracklets belonging to a same object.

	Object 1	Object 2	Object 3
Semi-major axis [km]	42164.2	42165.4	42164.6
Eccentricity [-]	0.00024	0.02030	0.00009
Inclination [deg]	0.01	0.11	2.02
$\Omega + \omega$ + M [deg]	0.035	0.031	0.023

Table 2: Keplerian elements of the three GEO objects considered in simulations

4. Orbit determination and refinement. For each cluster, we select one pair of tracklets sufficiently separated (see Section 2.3) and its associated initial orbit is considered the initial guess in a least-squares (LS) filter where all tracklets of the cluster are taken into account. Aberrant tracklets are rejected and the orbit is refined solving another LS problem. The criterion of aberrant tracklets is defined with an Euclidian distance to the corresponding *simulated tracklet* (computed from the determined orbit) weighted with the telescope noise; if this distance is sufficiently long (higher than 20, for example), tracklet is rejected.

4. METHOD ASSESSMENT

In this section we present results of the application of this method to simulated objects first and then to real data extracted from observations of TAROT telescope.

4.1. Application to simulated objects

Simulations have been carried out considering three objects in the geostationary ring (see Table 2). These objects are observed in three consecutive nights within an observation interval duration of 3 hours each night. The two last intervals starts 22 and 51 hours after first interval, respectively. Inside these intervals, we have 50% chance of having one tracklet every 10 minutes which is assigned to one of the three objects randomly. This procedure along with the measurement noise considered (1 arcsec in both angular coordinates) make each simulation different. Two of these simulations are hereafter presented, called GEO3_1 and GEO3_2. Observations characteristics are those of a typical TAROT working scheme. A test is performed beforehand in order to characterize the shape of the minimum loss function when an all-vs-all approach is considered for building up the tracklets pairs (see Figure 5). There is in total 30 observations (13 corresponding to object 1, 10 to object 2 and 7 to object 3). Thus, there are 435 possible tracklet pairs ($n \cdot (n-1)/2$ where n is the number of tracklets), of which 144 pairs correspond to tracklet of the same object. In view of Figure 5, we draw up the following considerations:

- Clouds of pairs of the same or different object are well separated when tracklets are taken in the same night, whereas these clouds to be partly mixed when tracklets are 1 or 2 nights separated. This fact is an evidence of a recurrent paradox when we tackle jointly the correlation and initial orbit determination : we can confidently correlate two close observations but the issued orbit is not very precise and, on the contrary, it is hard to correlate two distant observations but the computed orbit is, in general, of better precision.

- Singularity for a number exact of revolutions is present. We see the divergence of minimum loss function values around 1 and 2 sidereal days. This is related to the distorted topography of the loss function (see Section 2.2).

- Definition of the threshold L^* is not straightforward. If we set $L^* = 1$, we would consider 200 associations, including 63 false associations (31.5%). Whereas for $L^* = 0.1$, 48 association are considered, of which 8 are false (16.7%). We decide to set the former value as threshold for the upcoming simulations.

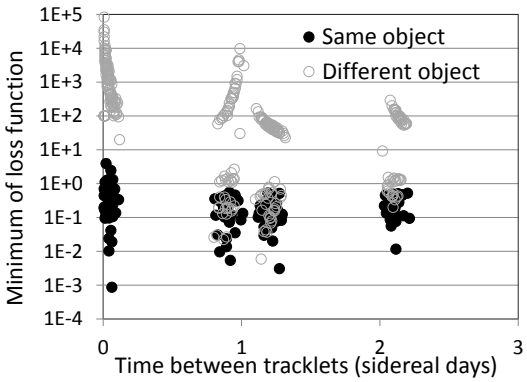

Figure 5: Minimum of loss function for all combinations of tracklets pairs coming from 3 geostationary objects

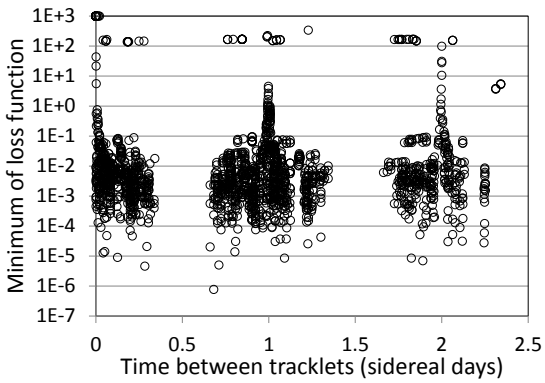

Figure 6: Minimum of loss function for all combinations of tracklets pairs in first three days of TAROT data

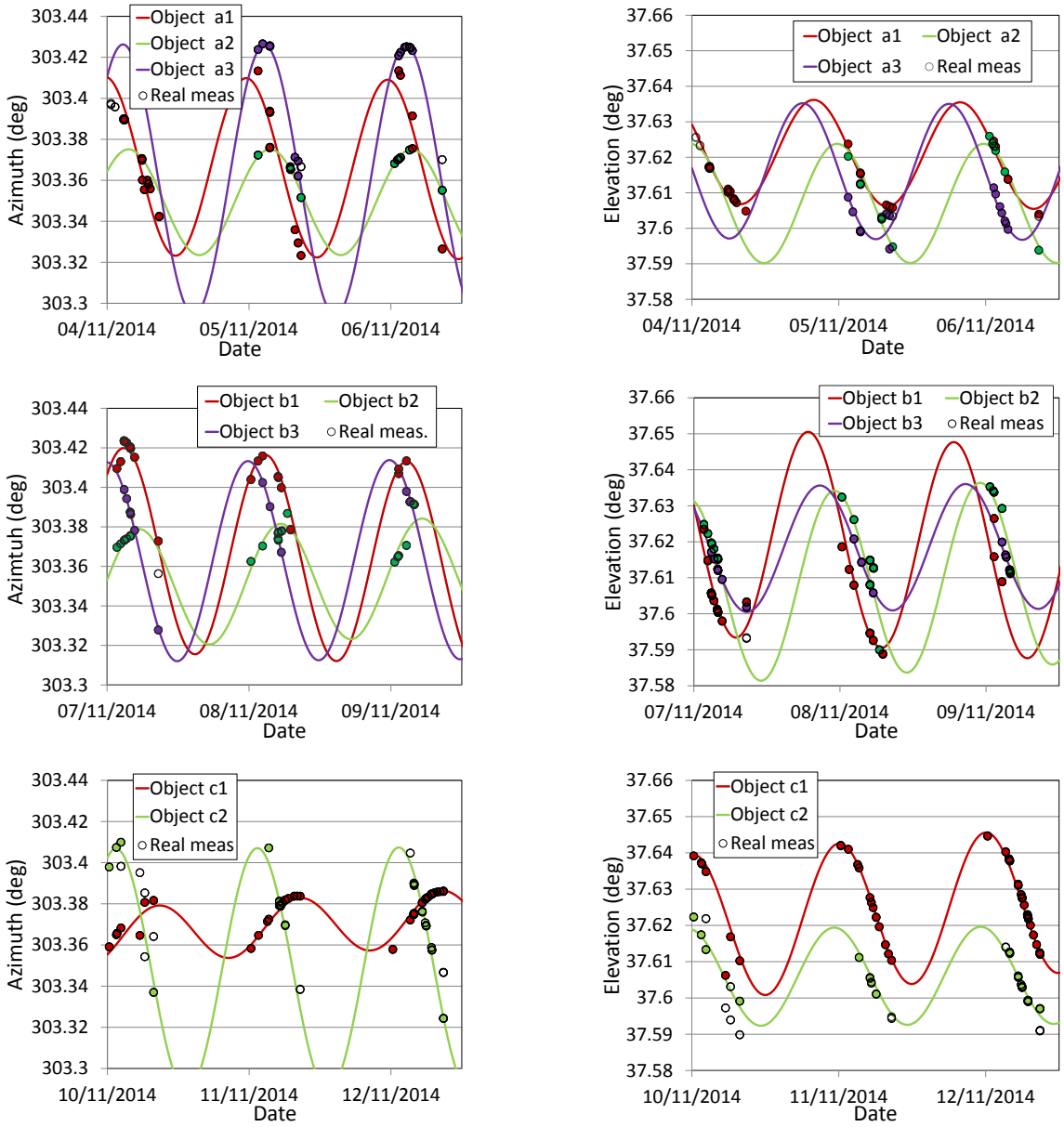

Figure 7: Correlation of real optical observations. Circles correspond to real observations, empty if they are not correlated to any object, full if they are correlated to the object of the same colour. Solid lines correspond to simulated observations of the identified objects.

In GEO3_1 simulation, the telescope takes 31 observations distributed 14, 7 and10 for objects 1, 2 and 3, respectively. There are 60 associations (7 false) that passes the threshold criterion concerning 27 of those 31 observations. A graph is then built up represented by a symmetric matrix of dimension 31×31. Markov clustering algorithm is then applied and three objects (clusters) are identified using 24 observations (distributed 11/6/7). There are two reasons for the 7 discarded observations in the clustering: 4 of them have no correlation relationship to any other, and 3 of them belonging to object 1 and taking within an interval of 30 minutes are densely associated to each other forming a separated cluster which is not considered because of its small size. These clustering results are stable for an inflation parameter in the range $(1.6, 3.0)$.

In GEO3_2 simulation, 30 observations are available distributed 8/10/12. There are 48 associations (3 false) that passes the threshold criterion concerning 24 observations. Markov clustering algorithm identifies 3 objects using 24 observations (distributed 7/8/7). Discarded observations come from observations that do not have correlation relationships (6) and observations that are involved in false associations (2). These clustering results are stable for an inflation parameter in the range $(1.8, 2.6)$.

In both cases, clustering algorithm succeeds to filter out false association, improving, in consequence, the objects identification. Similar simulations have been also performed with GTO and MEO objects[1] showing the same robust performance.

4.2. Application to real TAROT telescope observations

We have applied this method to observations taken by TAROT telescope located at Chile during 9 nights, from 4th to 12th November 2014. They point towards a sky region concerning the geostationary ring around a longitude of 107.3 deg W. At this longitude, three co-located geostationary satellites are orbiting. These satellites, part of the ANIK series, belong to the communications company Télésat Canada.

A total of 1223 optical observations are available. Association of these raw observations into tracklets is done with a linear correlator based on the Euclidian distance normalized to 3-sigma value. A group of observations are correlated only if this distance is below 0.1. We obtain 203 tracklets distributed as follows: 61 the first three days, 63 the following 3 days and 79 the last three days; that is to say, 609 *raw* observations out of 1223 are exploitable (49.8%). We apply the method to each interval of three days independently. It is worth noting that, in this real case, we do not differentiated clouds of pairs in Figure 6 for those tracklet of a same night. This feature complicates the choice of the loss function threshold, L^*. As we expect to identify at least three object and results from previous section, we set a threshold $L^* = 0.001$ that cuts off around 80% of combinations. In the first interval, 373 out of 1830 possible pairs are selected and we arrive to correlate 56 out of 61 tracklets (inflation parameter is set to 2.25). Tracklets from first days are only correlated to one object but in the next two days, correlation clearly identifies three objects as expected (see Figure 7). In the second interval, 548 out of 1953 combinations are selected and we arrive to correlate 62 out of 63 tracklets identifying, again, three objects. Inflation parameter is kept to 2.25. Comparing the objects obtained in first and second interval, we have differences of less than 250 m in semi-major axis, $5 \cdot 10^{-5}$ in eccentricity and 3 mdeg in inclination. Last interval is somehow different, there are more observations that in previous ones (+25%) and we can hardly see the presence of three objects as simultaneous three tracklets are only present in first day of this interval. There are 1135 out of 3081 possible pairs that pass the loss function threshold gate, what means 36.7% of the total, the highest percentage of the three intervals. This could be simply due to the fact of having, in principle, less objects at sight, so, more combinations contain tracklets of the same object. Two objects are only identified in this case using 64 out 79 tracklets (inflation parameter = 1.75). For visualize the goodness of the correlation, it is worth examining Figure 7 where simulated observations of the identified objects are plotted in each case, jointly with the real TAROT measurements and an indication of which observations have been correlated and used in the orbit determination.

[1] GTO object of study: sma$\simeq$ 24371 km, ecc$\simeq$ 0.73, inc$\simeq$ 4.0 deg
MEO object of study : sma$\simeq$ 29600 km, ecc$\simeq$ 0, inc$\simeq$ 56 deg

5. CONCLUSION

A robust procedure for processing uncorrelated tracks in the context of object identification has been presented. It mainly combines two methods: a method that provides an initial orbit and a correlation likelihood for a pair of optical tracklets and a clustering algorithm for object identification. First applications of this procedure are promising, showing good behaviour against false associations. Further investigations are also needed to determine criteria for setting the inflation parameter, analyzing the number of nights which is optimal to be considered as a function of the orbital regime and assess the case when data from multiple telescopes is available.

REFERENCES

1. Siminski J. A., et al., (2014). Short-arc tracklet association for geostationary objects, *Advances in Space Research* **53**, 1184-1194.
2. Weigel M., Meinel M. and Fiedler H., (2015). Processing of optical telescope observations with the space object catalogue BACARDI, *25th International Symposium on Space Flight Dynamics ISSFD*.
3. Milani A., et al., (2004). Orbit determination with very short arcs I. Admissible Regions. *Celestial Mechanics and Dynamical Astronomy* **90**, 57-85.
4. Thiebaut C., et al. (2004). CNES optical observations of space debris in geostationary orbit with the TAROT telescope: IADC campaign results. *35th COSPAR Scientific Assembly* **35** 984.
5. Izzo D. (2015) Revisiting Lamberts problem. *Celestial Mechanics and Dynamical Astronomy* **121** 1-15.
6. Schaeffer S. E. (2007) Graph clustering. *Computer Science Review* **1**, 27-64.
7. van Dongen S. (2000). Graph Clustering by Flow Simulation. *University of Utrecht*. Ph.D. Thesis.
8. Enright A. J., Van Dongen S., and Ouzounis C. A. (2002). An efficient algorithm for large-scale detection of protein families. *Nucleic acids research* **30(7)**, 1575-1584.
9. Dorow B., Eckmann J. P., and Sergi D. (2004). Using curvature and markov clustering in graphs for lexical acquisition and word sense discrimination. *Workshop MEANING-2005*.
10. Boyd S., and Vandenberghe L. (2004). Convex optimization. *Cambridge university press*.
11. DeMars K. J., Jah, M. K. and Schumacher P. W. (2012). Initial orbit determination using short-arc angle and angle rate data. *IEEE Transactions on Aerospace and Electronic Systems* **48(3)**, 2628-2637.